JCTC Journal of Chemical Theory and Computation

Mixed Resolution Modeling of Interactions in Condensed-Phase Systems

Sergei Izvekov and Gregory A. Voth*

Center for Biophysical Modeling and Simulation and Department of Chemistry, University of Utah, 315 South 1400 E., Room 2020, Salt Lake City, Utah 84112-0850

Received August 7, 2009

Abstract: A new mixed resolution method is developed for modeling molecular interactions that employs a distance-dependent coupling of atomistic and coarse-grained force fields. In the mixed resolution interaction (MRI) method, detailed atomistic structure is maintained over the whole system. However, the atomistic force field is used for close interparticle separations (called the atomistic zone), while at large separations the coarse-grained forces are "unfolded" into atomistic interactions in a way that reduces the cost of the simulation compared to standard long-range approximations or cutoff schemes. Several variations of the unfolding scheme are described. The method is applied to develop MRI models of bulk TIP3P water, based on one-site multiscale coarse-grained (MS-CG) water potentials located at the molecular centers of either mass or geometry. With a sufficiently large atomistic zone (>0.7 nm), the MRI models provide excellent simulations of the bulk water phase. MRI modeling is further illustrated for liquid methanol with both one- and two-site coarse graining. The MRI water models are then used to simulate aqueous solutions, where the solutes are treated at the atomistic level. It is shown that the MRI treatment significantly alters solute association dynamics if it relies on the MS-CG force fields obtained solely from the bulk phase. Possible modifications of the MRI procedure to improve the transferability of water potentials to heterogeneous systems are, therefore, discussed. The best result is obtained if water molecules within a preselected cutoff distance from the solute are described using only atomistic potentials. As a final example, the MRI method is applied to model a solvated phospholipid bilayer.

1. Introduction

The structure and dynamics of complex condensed-phase systems are often influenced by multiscale phenomena. It is possible to adequately describe the behavior of such systems on mesoscopic or macroscopic scales, although such models are necessarily less complete than those described by the full set of atomistic variables and the laws describing their interactions. The limited success and transferability of many empirical models, tailored to study condensed-phase systems on particular scales, testifies to this fact. The first and most widely used strategy for empirical modeling, which may be recognized as a top-down approach, is based on extracting dynamic variables and interactions directly from the system's mesoscopic properties. In contrast, the more recent bottom-up philosophy in condensed-phase modeling assumes that a hierarchy of relevant scales exists in condensed-phase systems, beginning with the molecular scale. The bottom-up approach first identifies the most important degrees-of-freedom on mesoscopic scales and then projects the atomistic coordinates and interactions onto the phase space spanned by the relevant coordinates. Such a strategy holds certain advantages over top-down strategies since explicit molecular-scale force information is systematically propagated upward in scale to the mesoscopic level. However, it is also technically more complex and, in some cases, may become infeasible because atomistic simulations are computationally expensive.

A simpler but potentially less accurate approach than the fully atomistic description is particle-based coarse graining,

* Corresponding author. Telephone: 801-581-7272. Fax: 801-581-4353. E-mail: voth@hec.utah.edu.

10.1021/ct900414p CCC: $40.75
Published on Web 11/03/2009

where groups of atoms are replaced by single interaction sites.[1] Particle-based coarse-grained (CG) simulations have become popular because they provide controllable, quasi-atomistic resolution and require significantly less computational cost than that of a fully atomistic treatment. While most particle-based CG methods rely on underlying atomistic structures to partition the system into interaction centers, strategies for coarse graining the interactions themselves have mainly been developed in the top-down spirit using thermodynamic information.[2−6] However, in recent years an efficient and systematic bottom-up strategy for constructing effective pairwise CG interactions has been developed that provides a mapping of the molecular interactions onto a pairwise decomposable many-body potential of mean force (PMF) in the CG coordinate space by matching the effective CG forces to the forces along fully atomistic simulations.[7−15] The method is called multiscale coarse graining (MS-CG) and has been applied to a variety of complex condensed-phase and biomolecular systems.[1]

In many instances, however, CG models are not sufficiently accurate so that atomistic or dynamics become necessary for some key part of the system. This fact has prompted the development of mixed resolution methods where the system is partitioned into different domains. In quantum mechanics/molecular mechanics (QM/MM) approaches, for example, a small subset of the system is treated quantum mechanically, while the rest is treated by a classical empirical potential. A common simplification in QM/MM, and in many mixed-resolution methods, is the prevention of particle exchange between domains. Such a restriction clearly limits the scope of their applications, for example by excluding systems with strong fluctuations and diffusive properties. Realistic modeling of particle flow across boundaries in a mixed-resolution representation requires the ability to adjust a particle's resolution as it moves across the predefined resolution boundaries. Several adaptive resolution (AdRes) schemes have recently emerged in response. The so-called "hybrid particle" in such schemes is represented by a weighted superposition of its various representations and interactions.[1,16−22] (The particle adopts its hybrid form only inside transition regions, which separate regions of different resolution.) The major feature distinguishing the various AdRes schemes is how interactions between domains of different resolutions are coupled in the transition region. In the potential-based AdRes method, effective forces are determined from a smoothly varying potential across the resolution transition region. In the force-based scheme, the reverse approach is adopted.

The present paper describes a significantly different strategy to couple CG and atomistic descriptions, which we call mixed resolution interaction (MRI) modeling. The general idea is to implement different resolution models depending only on the radial distance between the interacting particles. MRI modeling is based on the intuitively obvious fact that the interactions between sufficiently distant separated particles, belonging to the so-called "CG distance zone", should be well described by a lower resolution CG force field. As the particles move closer together, the CG force field should be smoothly replaced by a fully resolved atomistic force calculation. The overall MRI approach assumes that the CG forces can be mapped (or "unfolded") onto atomistic forces as two particles move out of the atomistic distance zone. It should be stressed that in the MRI method both resolutions (atomistic and CG) "live" throughout the entire simulation system. There are no resolution boundaries in real space.

The MRI force unfolding algorithm addresses the question of how a CG force, normally applied to the center-of-mass of an atomistic group (or more generally to the location of a CG site), should be distributed over individual atoms of the group. The solution to this problem is not unique, a fact that introduces some (unavoidable) ambiguity into the MRI method. The nonuniqueness of the unfolding scheme is associated with the inevitable loss of information incurred upon the coarse graining of a system.[1] However, the advantage of MRI modeling over the alternative of a pure CG simulation implemented at all length scales is that the MRI simulation limits the loss of information to primarily the long-range interactions. Fully atomistic resolution in the structure is preserved at short range, and these atomistic short-range interactions are maintained in every part of the system, also in contrast to the AdRes schemes.

In practice, the computational efficiency of the MRI method is defined by two factors: the size of the atomistic zone and the simplicity of the force unfolding algorithm. The atomistic zone should encompass all parts of the free energy surface that are "molecularly rough". Conversely, the atomistic interactions may be safely replaced by CG interactions in regions where the characteristic length scale of variations in the effective free energy surface (many-body PMF) begins to exceed the linear dimension of the CG groups. One possible criterion for the latter might be gleaned from the level of agreement between MS-CG potentials developed for two different choices of CG sites within the groups (e.g., center-of-mass vs geometrical center). Agreement between the two MS-CG effective potentials at some interparticle distance would indicate that the CG forces could be unfolded into atomistic ones at that distance in the MRI scheme. Note that because MRI potentials are pairwise, MRI modeling can be combined with accurate atomistic interactions in a selected subsystem, in principle allowing for an efficient way to simulate heterogeneous systems.

The following sections of this article are structured as follows. Section 2 begins with a summary of the MS-CG method and then presents an overview of the MRI method. In Section 3.1, the MRI one-site water model is described, and MRI simulation of TIP3P water in the bulk phase is presented. In Section 3.2, the same is done for liquid methanol. In Section 4, the MRI TIP3P water potential's transferability to heterogeneous systems is analyzed by simulating an aqueous sodium ion solution. Also in Section 4, the MRI method is applied to simulate a phospholipid bilayer. The paper closes with conclusions in Section 5.

2. Mixed Resolution Interaction Method

In essence, the MRI approach is a distance-dependent coupling of the atomistic and CG force fields, which must be chosen to be as consistent as possible. The best result can

be achieved if the CG interactions represent an ensemble average of the exact atomistic interactions projected upon the coarse-grained degrees-of-freedom. In this case, the configurationally averaged atomistic and CG interactions between distant molecules are close to identical. The MS-CG method, which has been extensively described elsewhere,[1,7,8,13−15] derives the effective CG interactions through a statistical mechanically consistent projection of the atomistic forces onto the CG space. It, thus, satisfies the above requirement.

2.1. MS-CG Interactions. Here we present a brief outline of the MS-CG method relevant to MRI modeling.[14,15] In the MS-CG approach, coarse graining of an n-particle Cartesian phase space ($\mathbf{r}^n$, $\mathbf{p}^n$) with a Hamiltonian $h(\mathbf{r}^n, \mathbf{p}^n)$ corresponds to mapping the coordinates of the n particles into N CG groups. This process is represented as a canonical coordinate transformation to a new phase space ($\mathbf{R}^N$, $\mathbf{P}^N$). The latter is spanned by the intragroup locations of the N atomic groupings:

$$\mathbf{R}_I(\mathbf{r}^n) = \sum_{i=1,s_I} c_{Ii}\mathbf{r}_i \qquad (1)$$

$$\mathbf{P}_I(\mathbf{p}^n) = \sum_{i=1,s_I} \mathbf{p}_i$$

where s_I is the number of atoms in the Ith grouping, and the coefficients c_{Ii} satisfy:

$$\sum_i c_{Ii} = 1 \quad \text{for } I = 1, ...,N \qquad (2)$$

Equation 2 ensures that the ($\mathbf{R}^N$, $\mathbf{P}^N$) coordinates are canonical. $\mathbf{R}_I$ and $\mathbf{P}_I$ will be the position and the momentum of the center-of-mass (CM) of the Ith group if $c_{Ii} = m_{Ii}/M_I$, where m_{Ii} is the mass of the i^{th} atom and $M_I = \sum_{i=1,s_I} m_{Ii}$ is the total mass of group I. Alternatively, the choice $c_{Ii} = 1/s_I$ is equivalent to the assumption that all atoms in the group have equal mass. In this latter representation, $\mathbf{R}_I$ is the geometrical center of the CG group.

The effective pairwise interaction Hamiltonian, which describes the canonical distribution in the CG phase space ($\mathbf{R}^N$, $\mathbf{P}^N$), is constructed to represent the all-coordinate exact CG many-body potential of mean force $U(\mathbf{R}^N)$. This can be achieved by introducing a pairwise approximation to $U(\mathbf{R}^N)$ into the CG Hamiltonian. A pairwise form ensures that the CG effective potential term can be expressed as the integral of a pairwise and, thus, the conservative approximate CG force field as

$$\mathbf{G}_{\mathbf{R}_I}(\mathbf{R}^N,\Omega) = \sum_{J\neq I} g(R_{IJ},\Omega)\mathbf{n}_{IJ} \qquad (3)$$

whose free parameters Ω are adjusted to approximate (in the least-squares sense) the all-coordinate CG many-body potential of mean force field:[1,15]

$$\mathbf{F}_{\mathbf{R}_I}(\mathbf{R}^N) = -\nabla_{\mathbf{R}_I} U(\mathbf{R}^N) \qquad (4)$$

In eq 3, R_{IJ} is the distance between CG groups I and J located at $\mathbf{R}_I$ and $\mathbf{R}_J$, respectively, and $\mathbf{n}_{IJ} = \mathbf{R}_{IJ}/R_{IJ}$ is the unit vector pointing from J to I. The pairwise MS-CG force field $\mathbf{g}_{IJ}(R_{IJ}, \Omega) = g(R_{IJ}, \Omega)\mathbf{n}_{IJ}$ is, thus, central and radially symmetric. As shown elsewhere,[14,15] if $\mathbf{G}_{\mathbf{R}_I}(\mathbf{R}^N, \Omega)$ [or the $\mathbf{g}_{IJ}(R_{IJ}, \Omega)$] is linear in Ω (i.e., if it can be expanded into a set of basis functions whose coefficients are the parameters Ω), then a least-squares fit to the mean net forces $\mathbf{F}_{\mathbf{R}_I}(\mathbf{R}^N)$ is equivalent to a least-squares fit to their instantaneous magnitudes $\mathscr{T}_{\mathbf{R}_I}(\mathbf{R}^N)$. The latter can be evaluated from an atomistic simulation as $\sum_{i=1,s_I}\mathbf{f}_i$, where the $\mathbf{f}_i$ are instantaneous net forces on individual atoms of the group. The least-squares problem is thereby reduced to a set of linear equations,[8,15] which can be solved using a block-averaging scheme.[7−9] A linear basis set can be conveniently constructed using piecewise functions, for example, a spline representation.[7−9,15]

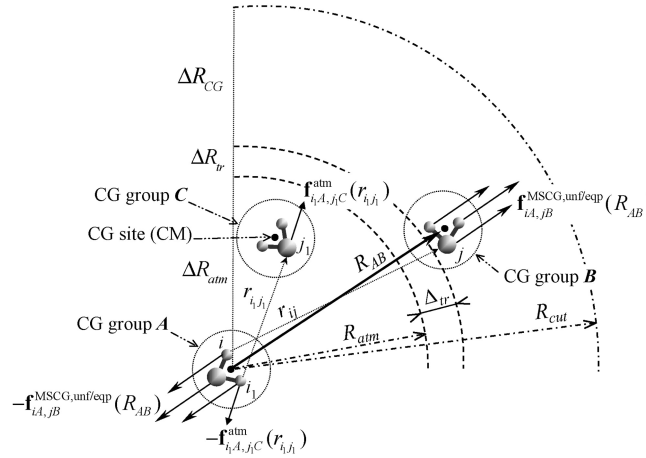

Figure 1. Schematic of the equipartition approach for evaluating pairwise atomistic contributions given the total MRI force acting between two CG groups (eqs 6, 9−11).

2.2. MRI-Coupling Atomistic and MS-CG Interactions. This section describes the mixed resolution force-based scheme employed to couple atomistic and MS-CG interactions. At the same time, it suggests a potential-based scheme, whose relation to the force-based scheme is similar to that seen in the AdRes methods.[22,23] While the force-based scheme is generally easier to implement, it does have a drawback related to the difficulty of defining a potential for the mixed (coupled) force field.

The location chosen for a CG site within the group is assumed here to be to as its CM, thus, assuming a proper distribution of atomic masses. The interval between two CMs is partitioned into three regions, as shown in Figure 1: the atomistic zone ΔR_{atm}; $R \leq R_{\text{atm}}$, the transition region ΔR_{tr}; $R_{\text{atm}} < R \leq R_{\text{atm}} + \Delta_{\text{tr}}$, and the CG zone ΔR_{CG}; $R_{\text{atm}} + \Delta_{\text{tr}} < R \leq R_{\text{cut}}$. The distance R_{atm} is the cutoff for the atomistic zone, while Δ_{tr} is the width of the transition region. The distance R_{cut}, the cutoff for the CG zone, is taken to be equal to the cutoff used for the MS-CG interactions.[15] The purpose of the transition region is to join smoothly the forces in the atomistic and CG regions.

The total force acting on the i^{th} atom in the k^{th} CG group of type α, with the latter two indices grouped as $A = (\alpha k)$, can be written as

$$\mathscr{T}^{\text{MRI}}_{iA}(r) = \sum_{j,B} \mathbf{f}^{\text{MRI}}_{iA,jB}(r, R_{AB}) \qquad (5)$$

The summation runs over all groups $B = (\beta l)$, $B \neq A$, whose atoms $(jB) = p$ act on the atom $(iA) = s$ with nonzero forces $\mathbf{f}_{sp}^{\mathrm{MRI}}$, given that the atoms s and p are separated by a distance r and the groups' CMs are R_{AB} apart. In the force-based scheme, the force between atoms s and p depends on which zone the intergroup separation $R = R_{AB}$ falls into

$$\mathbf{f}_{sp}^{\mathrm{MRI}}(r,R) = \begin{cases} \mathbf{f}_{sp}^{\mathrm{atm}}(r); & R \in \Delta R_{\mathrm{atm}} \\ \mathbf{f}_{sp}^{\mathrm{atm}}(r)w(R) + \mathbf{f}_{sp}^{\mathrm{MSCG,unf}}(R)(1 - w(R)); & R \in \Delta R_{\mathrm{tr}} \\ \mathbf{f}_{sp}^{\mathrm{MSCG,unf}}(R); & R \in \Delta R_{\mathrm{CG}} \end{cases} \quad (6)$$

In eq 6, $\mathbf{f}_{sp}^{\mathrm{atm}}(r)$ denotes the fully resolved atomistic force:

$$\mathbf{f}_{sp}^{\mathrm{atm}}(r) = \mathbf{f}_{sp}^{\mathrm{sr}}(r) + \mathbf{f}_{sp}^{\mathrm{coul}}(r), \quad (7)$$

where $\mathbf{f}^{\mathrm{sr}}$ is a short-ranged (e.g., Lennard-Jones) contribution, and $\mathbf{f}^{\mathrm{coul}}$ is the electrostatic (Coulomb) component. The symbol $\mathbf{f}_{sp}^{\mathrm{MSCG,unf}}(R)$ in eq 6 represents a pairwise atomistic interaction derived from the CG interaction between groups containing the atoms s and p, in accordance with the preselected unfolding algorithm for the pairwise CG force $\mathbf{f}_{AB}^{\mathrm{MSCG}} = \mathbf{f}_{\alpha\beta}^{\mathrm{MSCG}}(R_{AB})$ (the indices α and β denote kinds of groups). To make the $\mathbf{f}_{sp}^{\mathrm{MRI}}(r, R)$ force continuous everywhere, a smooth weighting function $w(R)$ is defined in the transition region with boundary conditions $w(R_{\mathrm{atm}}) = 1$, $w(R_{\mathrm{atm}} + \Delta_{\mathrm{tr}}) = 0$. We have adopted here the weighting function of the form $\cos^2(\pi(R - R_{\mathrm{atm}})/2\Delta_{\mathrm{tr}})$, which is similar to that used in ref 16. Such a weighting function implements a particularly simple way to ensure an interpolation between $w = 0$ and $w = 1$ that is monotonic, continuous, and differentiable and has a zero slope at the boundaries of the atomistic and (more importantly) the coarse-grained regions. Apart from these requirements the precise functional form is not especially relevant.

2.3. Unfolding MS-CG Interactions. In unfolding the MS-CG force $\mathbf{f}_{AB}^{\mathrm{MSCG}} = \mathbf{f}_{\alpha\beta}^{\mathrm{MSCG}}(R_{AB})$ into atom−atom contributions $\mathbf{f}_{iA,jB}^{\mathrm{MSCG,unf}}(R_{AB})$, where each contribution represents the force on atom (iA) due to atom (jB) at distance r_{ij}, the following constraint must first be satisfied:

$$\mathbf{f}_{AB}^{\mathrm{MSCG}} = \sum_{i,j} \mathbf{f}_{iA,jB}^{\mathrm{MSCG,unf}}(R_{AB}) \quad (8)$$

Of course, eq 8 alone is not enough. Additional assumptions regarding the directions and the amplitudes of the unfolded atomistic forces are required. First we will assume that:

$$\mathbf{f}_{iA,jB}^{\mathrm{MSCG,unf}} = f_{iA,jB}^{\mathrm{MSCG,unf}} \mathbf{e}_{ij}^{AB} \quad (9)$$

where $\{\mathbf{e}_{ij}^{AB}\}$ is a preselected set of unit vectors defining the possible directions of the unfolded forces. Newton's third law states that $\mathbf{e}_{ji}^{BA} = -\mathbf{e}_{ij}^{AB}$ and $f_{jB,iA}^{\mathrm{MSCG,unf}} = f_{iA,jB}^{\mathrm{MSCG,unf}}$. The latter two rules ensure that the Newton's third law is fulfilled all the time in the MRI simulation. The most natural choices of $\mathbf{e}_{ij}^{AB}$ point back and forth along the vector $\mathbf{r}_{ij} = \mathbf{r}_i - \mathbf{r}_j$ connecting the two atoms. However, such a choice would require an evaluation of the unique basis vector $\mathbf{e}_{ij}^{AB}$ for each pair of atoms and then inversion of the matrix $||(\mathbf{e}_{ij}^{AB} \times \mathbf{e}_{i'j'}^{AB})||$ to project the CG force $\mathbf{f}_{AB}^{\mathrm{MSCG}}$ onto the full basis $\{\mathbf{e}_{ij}^{AB}\}$. This approach would be computationally expensive. A simpler choice is to assume that all vectors in the basis have the same direction along the radius vector $\mathbf{R}_{AB} = \mathbf{R}_A - \mathbf{R}_B$, connecting the CMs of the two groups

$$\mathbf{e}_{ij}^{AB} = \mathbf{e}^{AB} = \mathbf{R}_{AB}/R_{AB} \quad (10)$$

A rule for how to project the $\mathbf{f}_{AB}^{\mathrm{MSCG}}$ force onto the vectors $\mathbf{e}^{AB}$ is still needed, as the latter is not linearly independent. An "equipartition" rule is probably the simplest choice, which distributes the MS-CG force equally over all atomic pairs:

$$f_{iA,jB}^{\mathrm{MSCG,unf/eqp}} = f_{AB}^{\mathrm{MSCG}}/(N_\alpha N_\beta) \quad (11)$$

where N_α and N_β are the numbers of atoms in the groups of type α and β, respectively, and f_{AB}^{MSCG} is the modulus of $\mathbf{f}_{AB}^{\mathrm{MSCG}}$. This rule is depicted in Figure 1. Calculating the force between the two CG groups by eqs 8−11 is, thus, $\sim N_\alpha N_\beta/2$ times faster than evaluating the short-ranged interactions for each pair (iA, jB).

The simplicity of the equipartition approach comes at a cost, however. First of all, it ignores the structure of the groups. For example, if any of the CG group atoms are charged, then the forces will not be consistent with the partial charge distribution over the group because interactions in the CG zone are mostly of an electrostatic origin. Second, the direction of the $\mathbf{f}_{ij}^{\mathrm{MSCG,unf}}$ force is always the same no matter how the groups are mutually oriented. Third, the unfolded forces can be noncentral, as the $\mathbf{R}_{AB}$ and $\mathbf{r}_{ij}$ vectors may be not collinear. The noncentrality of unfolded forces may lead to difficulties in introducing a corresponding potential energy, as will be discussed shortly.

Let us, thus, consider possible enhancements or alternatives to the equipartition algorithm, in particular approaches that better account for atomic partial charges and orientations, or those that yield central forces. One straightforward modification addressing the problem of atomic partial charge dependence would be to select the $\mathbf{e}_{ij}^{AB}$ vector, whose sign (direction) agrees with the product of the respective partial atomic charges $q_i q_j$. This modification to eq 11 leads to the unfolding rule:

$$\mathbf{e}_{ij}^{AB} = \mathbf{R}_{AB}/R_{AB} sgn(q_i q_j) \quad (12)$$

$$f_{iA,jB}^{\mathrm{MSCG,unf/coul}} = f_{AB}^{\mathrm{MSCG}} q_i q_j/(Q_\alpha Q_\beta)$$

where Q_α is the net charge of a group of type α. This change seems well justified in situations where the direction of the force between atoms at large separations is determined by the sign of their partial charge product $q_i q_j$.

The equipartition approach can also be made to depend on orientation by redefining the forces in the CG zone. We write $\mathbf{f}_{AB}^{\mathrm{MSCG}}(R_{AB}, \mathbf{d}_A, \mathbf{d}_B)$, where $\mathbf{d}_{A(B)}$ is a vector representing the orientation (e.g., dipole moment) of group $A(B)$. To be consistent with the generic MS-CG force field $\mathbf{f}_{\alpha\beta}^{\mathrm{MSCG}}(R_{AB})$, this function has to satisfy the condition $\langle \mathbf{f}_{AB}^{\mathrm{MSCG}}(R_{AB}, \mathbf{d}_A, \mathbf{d}_B) \rangle_{\mathbf{d}} = \mathbf{f}_{\alpha\beta}^{\mathrm{MSCG}}(R_{AB})$. In this context, the brackets represent a

configurational average over group orientations. The following form meets this condition:

$$\mathbf{f}_{iA,jB}^{\mathrm{MSCG}}(R_{AB}, \mathbf{d}_A, \mathbf{d}_B) = \mathrm{f}_{AB}^{\mathrm{MSCG}}/(N_\alpha N_\beta) D(R_{AB}, \mathbf{d}_A, \mathbf{d}_B) \tag{13}$$

where

$$D(R_{AB},\mathbf{d}_A,\mathbf{d}_B) = 2\delta d_{\mathbf{d}_A,\mathbf{d}_B}(R_{AB}) + 1 \tag{14}$$

In eq 14, the term:

$$\delta d_{\mathbf{d}_A,\mathbf{d}_B}(R_{AB}) = d_{\mathbf{d}_A,\mathbf{d}_B} - \langle d_{\mathbf{d}_A,\mathbf{d}_B}\rangle \tag{15}$$

represents the instantaneous deviation of the group orientation from its ensemble average. The first term is defined in terms of inner products of vectors as follows:

$$d_{\mathbf{d}_A,\mathbf{d}_B} = (\mathbf{d}_A,\mathbf{d}_B) - 3(\mathbf{d}_A,\mathbf{n}_{AB})(\mathbf{d}_B,\mathbf{n}_{AB}) \tag{16}$$

where the dipoles are separated by a distance R_{AB} and $\mathbf{n}_{AB}$ is a unit vector along the radius vector $\mathbf{R}_{AB}$. Indeed, eq 13 produces the desired configurational average because

$$\langle D(R_{AB},\mathbf{d}_A,\mathbf{d}_B)\rangle_{\mathbf{d}} = 1 \tag{17}$$

A factor of 2 was introduced in the definition of $D(R_{AB}, \mathbf{d}_A, \mathbf{d}_B)$ [eq 14] so that D can adopt positive or negative values. The $\langle d_{\mathbf{d}_A,\mathbf{d}_B}\rangle$ term can be calculated in advance, for example, by taking an ensemble average over the same atomistic trajectories and mesh that were used to obtain the MS-CG potentials. More generally, a number of different functions $D(R_{AB}, \mathbf{d}_A, \mathbf{d}_B)$ might be constructed for eq 13 which satisfy the condition in eq 17. This scheme is referred to as the dipole-disorder, or more simply, the dipole algorithm.

The last drawback of the equipartition algorithm, noncentrality of the unfolded forces, can be circumvented by assigning the force of eq 11 to only one pair of atoms: the i, j (i.e., $N_\alpha, N_\beta = 1$ and $\mathbf{e}_{ij}^{AB} = \mathbf{r}_{ij}/r_{ij}$) that lie closest to the CMs of their respective atomic groups. It is then assumed $f^{\mathrm{MSCG,unf}} = 0$ for the rest of the atom pairs. For example, in the case of water, the unfolding forces can be assumed to be nonzero only for the O−O pair. Such a scheme may be sufficiently accurate for systems with smaller CG groups, such as water molecules.

To summarize, we note that the MRI model described in this section can be viewed as a mixed resolution generalization of cutoff treatments where the long-ranged interactions depend on the charge (or neutrality) of the groups. The underlying idea is similar in that interactions between atoms are switched to CG interactions when the separation between two groups becomes larger than a predefined cutoff. They differ because the resolution of the interaction changes in the present MRI approach.

3. MRI Models of Bulk Polar Solvents

3.1. Water. The accuracy of MRI modeling will first be explored for TIP3P bulk water under ambient conditions ($T = 300$ K and $p = 1$ bar). The interactions in the CG zone are represented by one-site MS-CG potentials similar to those presented in ref 8. The reference system used to obtain the MS-CG interactions consisted of 512 molecules in a periodic, cubic volume simulated under constant *NVT* conditions and equilibrium density (1014.6 kg/m^3). Electrostatic interactions were treated using the Ewald summation method, and Lennard-Jones interactions were cut off at 1 nm. The configurations of this simulation were sampled each 0.1 ps, over a total of 100 ps. Two effective CG interactions were derived from the same atomistic trajectory/force data: one where the CG sites were located at the group CM, and another where they were located at the group geometrical centers (GC). MS-CG forces were determined using the block-averaging method on a linear mesh covering distances up to 1 nm, with a bin size of 0.005 nm. The result was insensitive to block size.

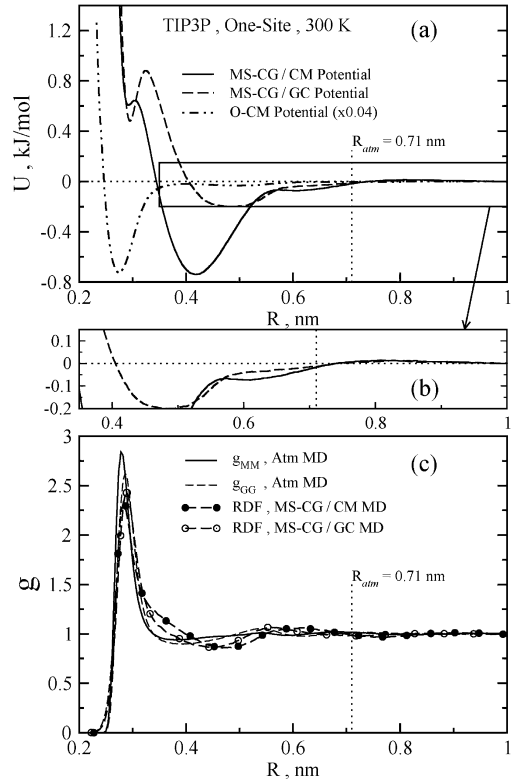

Figure 2. (a): One-site effective CG interactions associated with CM (solid), GC (dashed) sites for bulk TIP3P at ambient conditions and configurationally averaged interaction between an oxygen atom (O) and a water molecule scaled by a factor of 4×10^{-2} (dot-dashed). (b): Magnified tail region of potentials from (a). (c): CM and GC RDFs, g_{MM}, g_{GG} from the reference atomistic (solid and dashed, respectively), MS-CG/CM (filled circles), and MS-CG/GC (empty circles) simulations.

These two CG potentials, hereafter referred to as the CM and GC potentials $U_{\mathrm{CM}}^{\mathrm{MSCG}}$ and $U_{\mathrm{GC}}^{\mathrm{MSCG}}$, respectively, are shown in Figure 2. The same plot shows CM and GC radial distribution functions (RDFs) (denoted by g_{MM} and g_{GG}, respectively) derived from the reference atomistic MD and MS-CG simulations (the latter being lines labeled as "MS-CG/CM(GC)" in the legend). The RDFs resulting from the CG simulations are rather different from the structures seen in the reference atomistic MD simulation. The MS-CG/GC and atomistic g_{GG} RDFs exhibit a reasonably close match — the positions of the first and second solvation shells are well captured in the MS-CG simulation. The CM and CG

potentials also nearly coincide at short separations ($r < 0.285$ nm), that is, up to the position of the first peak in g_{MM} or g_{GG}. Their correspondence indicates that hydrogen bonding in a well-defined arrangement of interacting molecules is the dominant contributor to MS-CG potentials at these separations. Beyond the first peak, the molecular orientations become increasingly random causing the two potentials to differ. The CM and GC potentials also coincide at large ($r > 0.71$ nm, vertical-dotted lines in Figure 2) separations, that is, roughly the outer edge of the second solvation shell. The CM potential is substantially more attractive at intermediate distances, with a depth of almost -0.75 kJ/mol compared to -0.25 kJ/mol for the GC potential. The overall neutrality and small size of the water molecule implies a fast decay of the effective one-site interaction and also explains its insensitivity to the location chosen for CG sites at relatively short separations. In Figure 2a, we have plotted an effective interaction between an oxygen atom and a water molecule as a function of O−CM distance. The effective potential was obtained by averaging the O−H_2O potential energy over all configurations along the reference atomistic trajectories.

The CM and GC potentials start showing similarities at 0.71 nm, suggesting that this distance should be the size of the atomistic zone ΔR_{atm}. Due to agreement of the CM and GC MS-CG potentials at distances larger than 0.71 nm, one might expect that convergence of the properties in the MRI simulations can be reached with an atomistic zone radius R_{atm} larger than that distance. As will be discussed later, this is indeed the case. We, therefore, carried out MRI simulations using both MS-CG/CM and MS-CG/GC potentials and cutoff to the atomistic zone at $R_{atm} = 0.05$, 0.35, 0.5, 0.7, and 0.75 nm (the models are labeled MRI/CM(GC)/R_{atm}). All models used a transition zone of width $\Delta_{tr} = 0.1$ nm. We note that standard deviation of temperature in the *NVT* simulation for $R_{atm} = 0.7$ nm was similar to that found in the Ewald atomistic simulation (7.7 K). For $R_{atm} = 0.35$ nm, the standard deviation of temperature increased to 8.6 K.

The MRI/CM and MRI/GC models with almost no atomistic zone ($R_{atm} = 0.05$ nm), so that all interactions are unfolded from the MS-CG potential, performed very differently. The MRI/CM/0.05 simulation exhibited glassy dynamics, with overstructured RDFs (the first peak in g_{OO} is at 6.0), and a diffusion coefficient several orders of magnitude lower than the atomistic simulations predict. By contrast, the MRI/GC/0.05 simulation yielded accelerated dynamics, understructured RDFs (max $g_{OO} = 1.4$) and diffusions almost twice as fast as the fully CG MD simulation, or 10 times faster than the atomistic diffusion. The internal pressure was large and positive in both cases. Clearly, these results demonstrate that it is essential in the MRI method to have the atomistic zone of a sufficient size in order to achieve accurate results.

Figure 3 compares the structural properties (O−O RDFs) of TIP3P bulk water obtained from MRI simulations using other values of R_{atm} as well as the reference atomistic and the fully MS-CG data. The MRI simulations were run in the constant *NPT* ensemble for $R_{atm} = 0.7$ and 0.75 nm and run in the constant *NVT* ensemble for smaller values of R_{atm}. MRI/CM simulations produced a slightly worse liquid

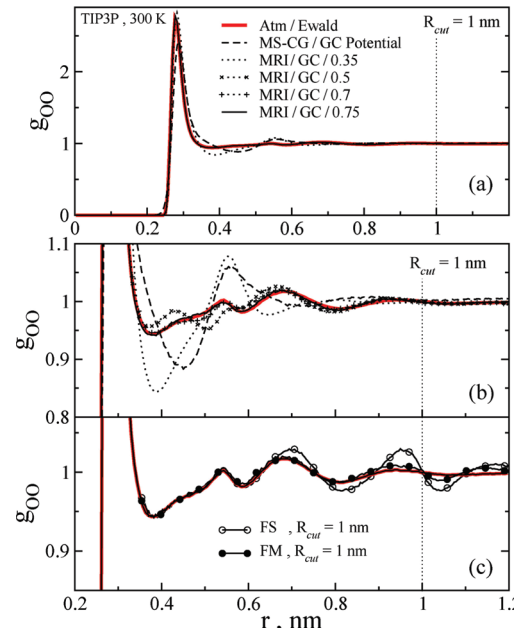

Figure 3. Comparison of the oxygen−oxygen structure in TIP3P water at ambient conditions, simulated with the atomistic Ewald (red), MS-CG/GC (dashed), and MRI/GC interactions. In the latter cases, various sizes of the atomistic zone are also shown: $R_{atm} = 0.35$ (dotted), 0.5 (crosses), 0.7 (pluses), and 0.75 nm (solid). (c) Atomistic Ewald and MRI structures are compared to an atomistic structure obtained using the FS (empty circles) and FM electrostatic descriptions (filled circles).

structure for $R_{atm} \leq 0.5$ nm, a direct consequence of the less-accurate structure produced by the MS-CG MD simulation with the bare CM potential (see Figure 2). Diffusion coefficients and some other thermodynamic properties from the MRI/CM and MRI/GC simulations are summarized in Table 1. All MRI models accurately modeled the first solvation shell, but the structure, dynamics, and thermodynamic properties of the liquid only became good as R_{atm} approached 0.71 nm (i.e., the distance beyond which the CM and CG potentials begin to coincide, cf. Figure 2b). As can be seen from the data shown in the Supporting Information (Table 1S), simulations using the Coulomb and dipole unfolding schemes for $R_{atm} > 0.7$ nm performed similar to the equipartition unfolding. At smaller values of R_{atm}, the dipole unfolding scheme in the constant *NVT* simulation yielded a slightly better structure and dynamics compared to those of the equipartition and Coulomb schemes. Unfortunately, including orientation-dependent interactions in the CG zone via dipole unfolding did not improve the pressure-related properties of the liquid.

Figure 4 shows the distribution of the three-body orientational order parameter:

$$q = 1 - \frac{3}{8}\sum_{j=1,3}\sum_{k=j+1,4}\left(\cos \mathrm{O}_j\mathrm{O}_i\mathrm{O}_k + \frac{1}{3}\right)^2 \qquad (18)$$

where $O_jO_iO_k$ is the angle formed by the oxygens of a central molecule and two of its four closest neighbors.[24] The average $\langle q \rangle$ is a measure of tetrahedral order, where a value of 1 indicates a perfect tetrahedral network and a value of 0 indicates uncorrelated particles. The MRI models whose

Table 1. Properties of Bulk TIP3P Water at Ambient Conditions[a,b]

model, R_{atm}(nm)	atm	0.35	0.50	0.70	0.75
N_{sol}/min g_{OO}	7.2/0.377	6.4/0.363	6.8/0.368	7.2/0.377	7.2/0.377
		7.9/0.388	6.53/0.368	7.2/0.377	7.2/0.377
$\rho(\delta\rho)$ [kg/m^3]/P (bar)	1014.6(11.8)/3.7	.../−1658.4	.../−915.9	1019.1(12.0)/3.7	1015.6(11.8)/3.7
		.../+641.0	.../−687.3	1020.0(12.0)/3.7	1015.1(11.8)/3.7
D_s (10^{-9}m^2/s)	5.3	6.3	5.7	5.4	5.4
		8.1	5.5	5.4	5.4
$U^{conf}(\delta U^{conf})$ [kJ/mol]	−41.1(0.3)	−44.8(0.4)	−45.2(0.4)	−45.9(0.4)	−45.9(0.4)
		−43.0(0.4)	−45.2(0.4)	−46.0(0.4)	−46.0(0.4)
κ_T (10^{-5} bar^{-1})	4.9	–	–	5.0	4.9
		–	–	5.0	4.9

[a] As determined from atomistic MD (atm) with Ewald summation and MRI simulations for various atomistic zone sizes R_{atm}. [b] Among the MRI models (columns three through six), the first line is for center-of-mass CG sites (MRI/CM), and the second is for geometrical center CG sites (MRI/GC). The properties shown are N_{sol}/min g_{OO}, [number of molecules in first solvation shell]/[first minimum in g_{OO}]; $\rho(\delta\rho)/P$, [density]/[equilibrium pressure], where the standard deviation of density is shown in parentheses if the constant *NPT* ensemble is used, and the symbol "..." denotes that the constant *NPT* was not used. Additional tabulated results are: D_s, the self-diffusion coefficient; $U^{conf}(\delta U^{conf})$, the average configuration energy per particle (and its standard deviation in parentheses); and κ_T, the isothermal compressibility.

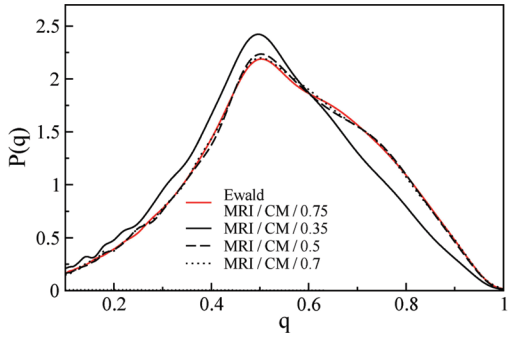

Figure 4. Distribution of the order parameter q, $P(q)$ from eq 18, from the atomistic Ewald (red) and MRI/CM simulations with $R_{atm} = 0.35$ (solid), 0.5 (dashed), 0.7 (dotted), and 0.75 nm (also red). The last is essentially identical to the exact Ewald simulation.

atomistic zones extend beyond the radius of the first solvation shell accurately reproduce the atomistic q distribution (giving values of $\langle q \rangle = 0.63$ for both the atomistic Ewald and MRI/0.75 simulations). In the simulation with $R_{atm} = 0.35$ nm, a distance which just reaches the first solvation shell, the distribution of q shifted to smaller values ($\langle q \rangle = 0.52$). This result suggests a decreased probability of finding nearest neighbors arranged tetrahedrally and, thus, suggests a softer hydrogen bonding. As reported in one of our previous papers,[25] adding a cutoff radius to the electrostatic interaction with force-shifted potentials does not affect the distribution of q for TIP3P water. However, a short-ranged model developed using the inverse MC method[26] appears to be much less accurate than MRI models with $R_{atm} > 0.7$ nm.

Another informative quantity is the deviation between the MRI and atomistic force fields, in terms of the total force acting on each atom in a configuration. Figure 5a shows the time evolution of the ratio between the Euclidean norm of this deviation and the atomistic force:

$$\Delta F = \frac{\left(\sum_{I \in \text{conf}} \|F_I^{\text{cutoff}} - F_I^{\text{Ewald}}\|\right)^{1/2}}{\left(\sum_{I \in \text{conf}} \|F_I^{\text{Ewald}}\|\right)^{1/2}} \qquad (19)$$

where the sum is over all atoms in the configuration. On the same plot, the ratio ΔF is evaluated for simulations using two cutoff electrostatic potentials:[25] one using a force-shifted (FS) and the other using a force-matched (FM) correction with $R_{cut} = 1.0$ nm. (The FM correction is a short-ranged representation of Ewald electrostatics, obtained through force-matching Ewald trajectories in the bulk SPC/E water under ambient conditions.)[25] Even for the MRI potential with an atomistic zone as large as 0.75 nm, the average error in the MRI forces is 3.5 times larger than that of the error produced with FS electrostatics. Figure 5b shows the relative contribution of the unfolded to the total forces in MRI models with various R_{atm} values and unfolding schemes. The CG contribution is consistently small: for the equipartition scheme, it is 8×10^{-3} at $R_{atm} = 0.3$ nm and less than 1×10^{-3} at $R_{atm} > 0.7$ nm. The constant *NPT* simulation with a neutral group-based cutoff, however, produces significantly denser water (by about 2−3%) than the Ewald simulation. This error noticeably and adversely affects the liquid structure, but surprisingly the diffusion rate is close to the atomistic value. In the constant *NVT* simulation at the Ewald equilibrium density, diffusion slowed to 4.7×10^{-9} m^2/s. The MRI potential with $R_{atm} = 0.7$ nm, however, reproduced the target density to within 0.4−0.5%, and the rate of self-diffusion to within 2%. The results further improved with the MRI/0.75 model, as seen in Table 1. These observations highlight the importance of a repulsive component to the effective one-site MS-CG potentials at distances $R > 0.7$ nm (see Figure 2b), which is absent from the effective interactions that ignore many-body correlations, such as group-based cutoffs.

3.2. Methanol. In this section, we consider one-site and two-site MS-CG models of liquid methanol (CH_3OH), similar to those reported in ref 8. A one-site MS-CG model with the CG site assigned to the molecular CM was previously shown to capture the structure of liquid methanol far better than that of a similar CG treatment of water.[8] A two-site model mapping the OH and CH_3 groups to CG sites also yielded good structural properties.

The reference atomistic simulation consisted of 125 MeOH molecules at $T = 300$ K in the constant *NVT* ensemble, contained in a box having 2.048 nm side lengths, and equilibrated for 2 ns. The interactions were modeled using Ewald electrostatics and the OPLS-AA force field,[27] which

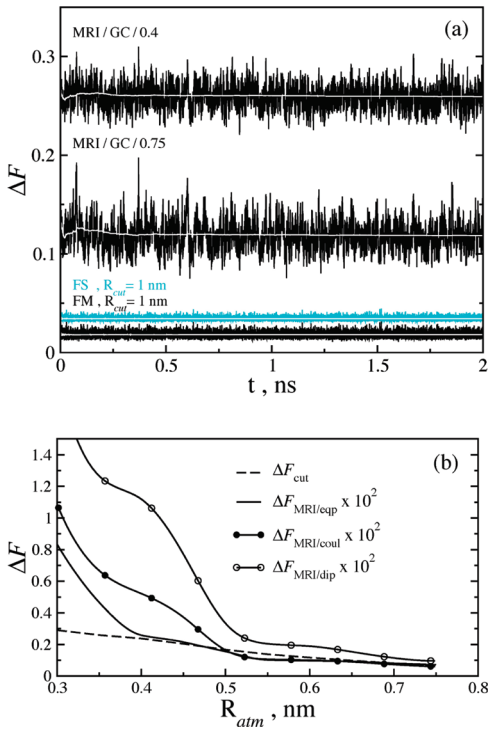

Figure 5. (a): Time evolution of the relative error ΔF in the Euclidean norm of the net forces (eq 19), resulting from MRI interactions with various atomistic zone cutoffs, compared to fully atomistic interactions. The net forces on each atom in the simulation at a given time step of the simulation are summed in calculating this error, and the atom trajectories are determined using a fully atomistic scheme. Data are also shown for reference atomistic simulations using the FS and FM description of electrostatics. The white lines show running time averages of each quantity. (b): Relative average contributions of the unfolded MS-CG/GC forces to the total forces using equipartition (solid), Coulomb (filled circles), and dipole (open circles) unfolding schemes.

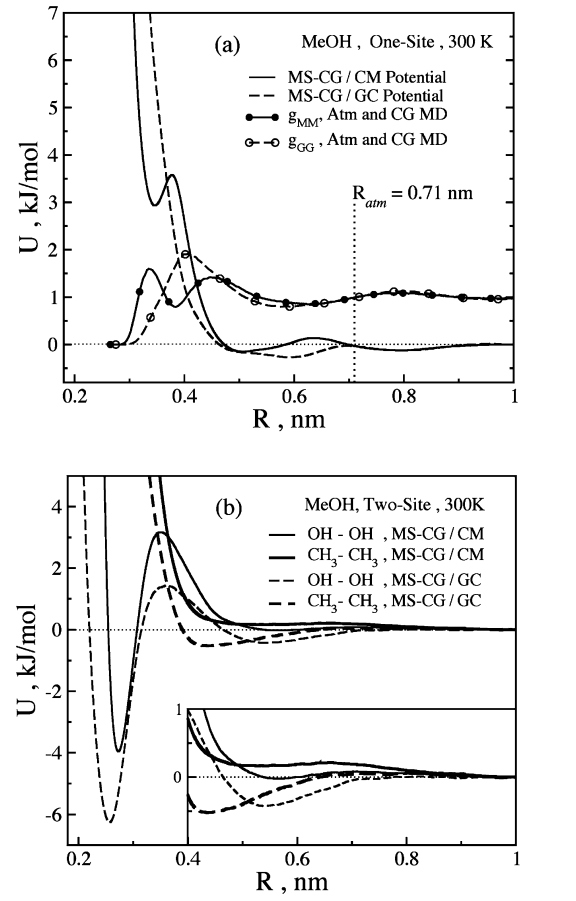

Figure 6. One-site (a) and two-site (b) MS-CG effective interactions associated with the CM (solid) and GC (dashed) sites for bulk MeOH at ambient conditions. The CM and GC RDFs from the reference atomistic and MS-CG (filled and empty circles) simulations are depicted in arbitrary units for one-site coarse graining.

is six site and flexible. The MS-CG procedure was essentially the same as for the water system. Figure 6a compares the effective MS-CG one-site interactions between molecular CMs and between GCs. The MS-CG/CM and MS-CG/GC force fields produced virtually identical RDFs to the reference atomistic RDFs (g_{MM} and g_{GG}, in arbitrary units, are presented in the same figure).

As the MeOH molecule is polar, one might expect that the effective one-site MS-CG interaction is insensitive to location of CG site at sufficiently large separations. As seen in Figure 6a, this is indeed the case. The MS-CG/CM and MS-CG/GC potentials both decay rapidly out to about 0.5 nm, exhibit substantial differences in the intermediate region, and then become indistinguishable (within the tolerance of the MS-CG procedure) at $R = 0.71$ nm. This threshold is surprisingly close to that of the water one-site model. By contrast, the MS-CG CM and GC interactions in a two-site representation, shown in Figure 6b, differ at all distances within 1.0 nm because the OH and CH_3 groups are charged and because the interaction between them decays less rapidly with distance.

For the one-site potentials, the structures generated by the MRI/CM and MRI/GC potentials improved progressively for larger values of R_{atm}, as demonstrated in Figure 7. The reason for the convergence of the properties is the agreement between the CM and GC one-site MS-CG potentials at distances larger than 0.71 nm, as discussed earlier for the case of water. For $R_{atm} = 0.75$ nm, the structure was virtually identical to the atomistic case. In contrast with water, however, the one-site methanol MRI potentials failed to reproduce the reference diffusion and internal pressure (and, therefore, density) as shown in Table 2. Diffusion in the MRI/CM/0.75 simulation was about 1.5 times faster, and the density was about 3.7% higher (if an isothermal compressibility of 12.2×10^{-5} bar^{-1} is assumed). However, the equilibrium pressure was positive in the MRI/CM/0.5 simulation and negative in the MRI/CM/0.75 simulation. One possible explanation for the difficulty with pressure reproduction in the MRI simulation is a large size of the MeOH molecules, as compared to water. Thus, an intermediate value of R_{atm} would reproduce the correct density in the MRI simulation.

4. Atomistic/MRI Modeling: Solutes in MRI Water

In terms of geometry and charge distribution, the MRI effective potentials are expected to be short ranged for small, neutral groups. In principle, to simulate a system containing

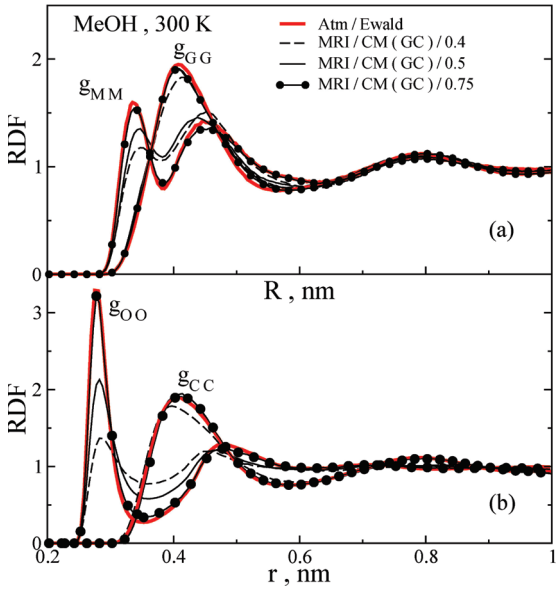

Figure 7. Comparison of the CM−CM structure (a) and atom−atom structure (b) in the liquid MeOH at ambient conditions, simulated with the atomistic Ewald (red) and MRI models with various sizes of the atomistic zone: $R_{atm} = 0.4$ (dashed), 0.5 (thin solid), and 0.75 nm (filled circles).

Table 2. Properties of Bulk Liquid Methanol at Ambient Conditions[a,b]

model, R_{atm} (nm)	atm	0.40	0.50	0.75
P (bar)	6	5 386	2 587	−302
D_s (10^{-9} m^2/s)	2.31	9.35	5.05	3.36

[a] As determined from atomistic MD (atm) with Ewald summation and one-site MRI/CM simulations with various atomistic zone sizes R_{atm}. [b] The atomistic simulations were in the constant *NPT* ensemble, while the MRI simulations were in the constant *NVT* ensemble at equilibrium atomistic density (773.7 kg/m^3). The properties listed here are P, the equilibrium pressure, and D_s, the self-diffusion coefficient.

charged species/groups, the MRI description may be introduced for neutral species, while the rest are treated on the atomistic level. In water solutions, for instance, the water−water interaction can be modeled using MRI, while the water-solute and solute−solute interactions are described atomistically. Such a description would be especially justified for bulky or charged solutes in solvents, such as water with low molecular weight. In many systems, such as biomolecular simulations, solvent−solvent interactions are the most computationally intensive aspect of the model. In such cases, MRI modeling of water may substantially increase simulation efficiency.

As the water and methanol examples have shown, MRI modeling is more efficient in scenarios where the effective intergroup interactions decay faster. Rapid decay is indicative of dominant high-order terms in the multipole expansion. The two lowest order multipole potentials, those between point charges and between a point charge and a dipole, are both long range. In the periodic simulation geometry, they even contain contributions from infinitely remote particles via the Ewald summation. The MRI formalism may, therefore, be less accurate in describing low-order interactions. This issue will now be explored.

4.1. Aqueous Ionic Solutions. As an example of such a mixed description, we now consider an aqueous ionic solution. The water−water interaction can be efficiently treated using the MRI formalism with an adequately large atomistic zone, as discussed in Section 3.1. Each ion is also a simple group but charged, so water−ion and ion−ion interactions have to be treated atomistically. Use of the MRI water−water interaction implies that ion−water electrostatics should also be evaluated using an approximate scheme, such as cutoff electrostatics. The latter requirement holds further for the ion−ion interaction, as the ionic subsystem is charged. In the mixed atomistic/MRI models reported here, we, thus, used an electrostatic potential with a FM correction[25] of $R_{cut} = 0.9$ nm. The FM correction has been shown to be transferable to different water models, thermodynamic conditions, and aqueous solutions, outperforming conventional cutoff treatments, such as (damped) force-shifted potentials.[25]

Two ionic solutions with approximately the same concentration were simulated. The first consisted of 4 sodium ions in 512 TIP3P water molecules, and the second had 12 ions in 1500 TIP3P molecules. The simulation volumes were periodic cubes of edge length 2.476 and 3.543 nm, respectively. In the reference atomistic simulations, carried out under constant *NVT* conditions, electrostatics were evaluated for the whole system using the Ewald method. In high-dielectric solvents, such as water, ionic charging free energies calculated by Ewald summation are largely invariant to the system size.[28] The use of counterions to maintain the charge neutrality of the system is, therefore, not necessary. In the atomistic/MRI model, the water−water interaction was described using various MRI/GC potentials with atomistic zones up to $R_{atm} = 0.75$ nm in size. Note that the bulk properties of water are well reproduced by the $R_{atm} = 0.75$ nm model, as discussed earlier.

The water solvation structure of the ion was reproduced accurately by the mixed MRI/atomistic simulation, as can be seen in the Supporting Information (Figure 1S). The only difference was a slightly overstructured first solvation shell: max $[g_{Na^+-O}] = 7.2$ in the MRI model compared to 6.9 in the fully atomistic Ewald simulation. This small difference is likely a consequence of our use of cutoff electrostatics in the atomistic interaction set for the mixed simulation. Despite the good structure of the MRI water, the structure of ionic association was drastically altered. Figure 8a compares the ion−ion RDFs of the reference atomistic and MRI/GC water simulations. In the latter, the ions show an excessive tendency to aggregate, which grew progressively stronger for smaller values of R_{atm}. Figure 8b shows the effective solvent-free ion−ion potentials, obtained using the MS-CG method. The results are similar to the all-site MS-CG potentials and, like them, can be interpreted as an approximate pairwise decomposition of the all-ion PMF. For complexes of two ions, the solvent-free ionic MS-CG potential is simply a pairwise PMF.

In the MRI water simulation with $R_{atm} = 0.4$ nm, the ions organized into a close-packed structure with a binding energy of −17 kJ/mol. After rapid formation of the ionic complex, they remained confined within a distance of about R_{atm} for the rest of the simulation. Even in the MRI water simulation

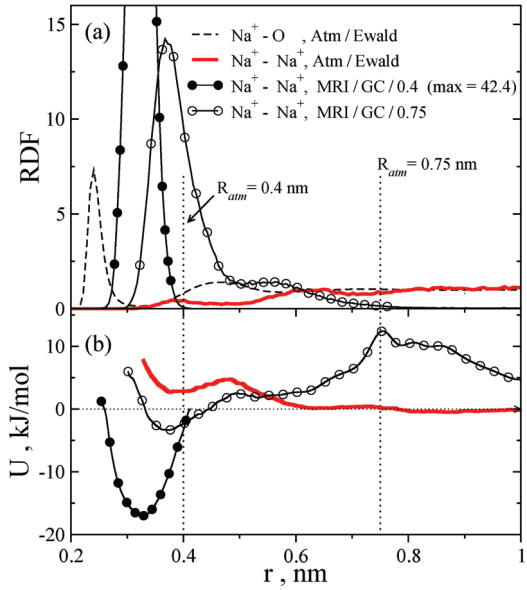

Figure 8. Simulations of ions in water. Results are shown for a simulation with 4 Na^+ ions and 512 H_2O molecules. (a): Ion−ion RDFs from atomistic Ewald MD (red), MRI/GC water with $R_{atm} = 0.4$ nm (filled circles), and $R_{atm} = 0.75$ nm (empty circles) simulations. The atomistic oxygen structure around the ions is also plotted (dashed line) as a reference. (b): Corresponding many-body MS-CG ion−ion effective interaction potentials.

with $R_{atm} = 0.75$ nm, the effective ion−ion interaction was significantly more attractive than that of fully atomistic data, with a globally stable contact minimum of −3.3 kJ/mol. The position of the minimum (0.38 nm), however, is close to the metastable contact minimum of the atomistic effective potential. The ion−ion effective interaction in the MRI/GC/0.75 water solution exhibits a high barrier with a maximum at about R_{atm}. A similar feature is probably present in the MRI/GC/0.4 model, but it could not be verified as the region outside R_{atm} was undersampled. In the reference atomistic simulation, the ion−ion effective interaction almost vanishes at distances of about 0.6 nm.

A possible origin of such behavior is explained in Figure 9. The unfolded CG interaction between water molecules is an approximation to the atomistic water interaction in bulk (between molecules W_1^{blk} and W_2^{blk} in Figure 9). Meanwhile, structural correlations between water molecules inside and outside the neighborhood of a solute (i.e., the region within R_{cut} of a solute) will be strongly perturbed by the presence of a charge (for example, between $W_{1(2)}^{slt}$ and W_1^{blk}). Thus, interactions in the perturbed zone of the water−water environment may be not adequately represented by the unfolded CG bulk interaction. This may lead to a more complex solvation structure and, therefore, different solute association dynamics.

The simplest remedy for the spurious, excessive segregation behavior is to describe the interactions between water molecules from the R_{cut}^{slt} neighborhood (denoted $W_{1(2)}^{slt}$ in Figure 9) and between all other molecules within R_{cut}, including those from the "bulk" (e.g., $W_{1(2)}^{slt}$−W_1^{blk} interactions), using the atomistic force field. The interaction between solvent molecules, if both are outside the R_{cut}^{slt} solute region (e.g., between the W_1^{blk} and W_2^{blk} molecules), can be safely

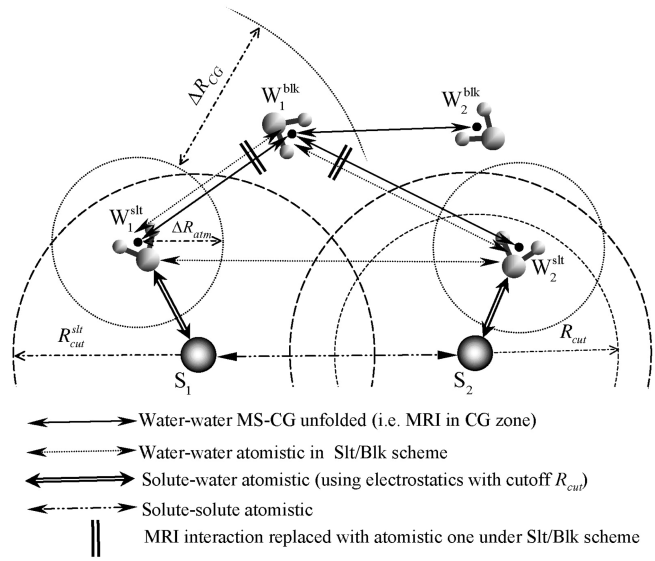

Figure 9. Schematic description of the slt/blk scheme for a treatment of water−water interactions in the MRI water ionic solution.

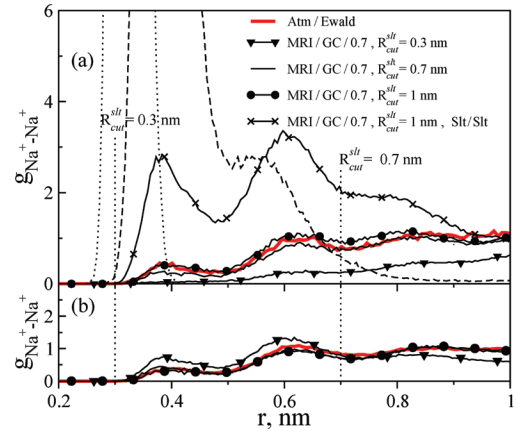

Figure 10. Ion−ion structure for the same system (a), shown in Figure 8, and for a simulation with 12 ions in 1 500 H_2O molecules (b). Both systems use the MRI/GC/0.75 model and the solute/bulk (slt/blk) scheme for water−water interactions (see Figure 9), with $R_{cut}^{slt} = 0.3$ (triangles), 0.7 (thin solid), or 1.0 nm (circles). The solid line with crosses is for an MRI simulation using the solute/solute (slt/slt) scheme, with $R_{cut}^{slt} = 1.0$ nm. The dotted and dashed lines, which correspond to the purely MRI modeling results shown as filled circle and empty circle lines from Figure 8, respectively, are shown for a comparison.

treated using the MRI formalism. Since the computational efficiency of such a treatment increases with the ratio of: (a) the number of water pairs formed by the bulk water molecules to (b) the number of pairs in which at least one molecule is within R_{cut}^{slt} of the solute species, the suggested approach is suitable for systems with a large bulk water subsystem (e.g., biological molecules in water). This idea is referred to as the solute/bulk (slt/blk) scheme. Figure 10 shows the ion−ion structures of MRI simulations running under the slt/blk scheme. For $R_{cut}^{slt} = 0.7$ nm, the ionic association dynamics were essentially identical to the fully atomistic. In the 12-ion slt/blk MRI simulation with $R_{cut}^{slt} = 0.3$ nm, the ion−ion structure was reproduced with almost

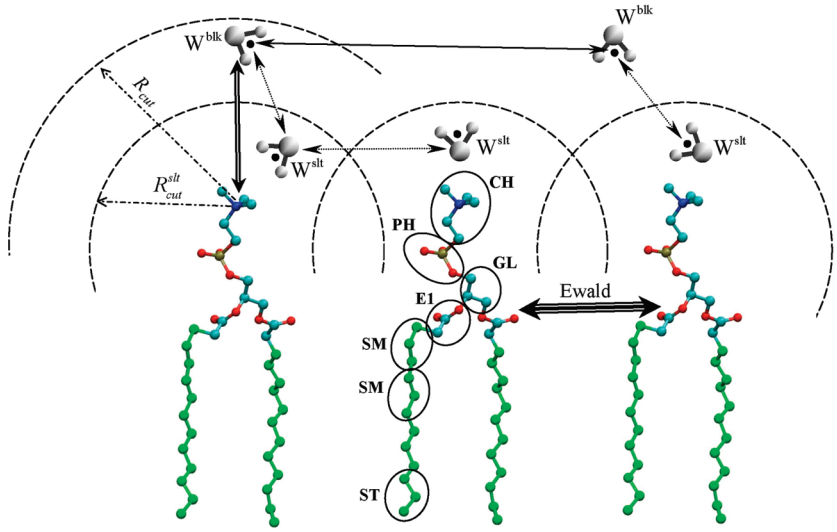

Figure 11. A schematic model of the interactions used in the simulating a DMPC bilayer in MRI water, with the slt/blk treatment of water molecules at the interface. Line legend is same as in Figure 9.

atomistic quality, while in the 4-ion system with $R_{cut}^{slt} = 0.3$ nm, the structure was somewhat worse. In the 4-ion simulations under the slt/blk scheme, ionic diffusion was 1.05(0.01) $\times 10^{-9}$ m^2/s for $R_{cut}^{slt} = 0.7$ nm but attained 1.18 $\times 10^{-9}$ m^2/s for $R_{cut}^{slt} = 1.0$ nm. The latter almost exactly matches the atomistic MD value of 1.20 $\times 10^{-9}$ m^2/s. The same tendency was observed in the 12-ion simulations.

It could be argued that the slt/blk scheme goes too far in its atomistic treatment of water−water interactions, as the association dynamics of solutes are governed mainly by interactions between water molecules from the ionic solvation shells (note that it might be better to say "within the R_{cut}^{slt} interaction shells"). However, it could be sufficient to accurately evaluate only interactions between pairs of water molecules that both lie within R_{cut}^{slt} of the solute. This scheme, referred to as solute/solute (slt/slt), is certainly computationally cheaper. Unfortunately, as demonstrated in Figure 10a, the ion−ion structures are different under the slt/blk and slt/slt schemes. A simulation with slt/slt enhancement of the MRI water−water interactions yielded better solute dynamics than one without, but the structure was still significantly different from the fully atomistic results. In particular, excessive contact (first peak in the RDF) and solvent-separated (second peak) pairs were still apparent in the ionic solute RDFs. The best results were, therefore, produced by the slt/blk approach.

4.2. Lipid Bilayer System. In this section, the MRI water model coupled with the slt/blk algorithm is applied to a phospholipid dimyristoylphosphatidylcholine (DMPC) bilayer. The bilayer was represented by 64 DMPC molecules and by 1 312 water molecules, corresponding to a hydration of 21 H_2O per DMPC. The DMPC molecules were modeled using a united atom atomistic force field.[29] This simulation used the rigid TIP3P water model with Lennard-Jones interactions for the hydrogen atoms set to zero. Electrostatic interactions were calculated via the particle-mesh Ewald (PME) summation.[30] The initial configuration was taken from ref 31 and then equilibrated for 20 ns in the constant *NPT* ensemble.

The bilayer geometry represents an infinite polarized interface between lipids and water, so the electrostatic contribution to configurational energy within the monolayer scales as $1/R_{cut}$ at distances greater than the cutoff R_{cut}. The effective FM electrostatic interaction in disordered water solutions decays much faster.[25] As discussed in the literature,[32] introducing a cutoff in the electrostatics may affect interactions between the normal components of headgroup dipoles. This issue could be a major factor, potentially affecting bilayer properties, such as surface equilibrium area and structure. It is, thus, best to treat the electrostatic interactions between lipids as accurately as possible, using the Ewald or PME methods. On the other hand, it has been noted that the effect of a cutoff on the bilayer properties is *less* important if the bilayer is properly hydrated (probably >27−28 molecules per lipid), and that, with proper hydration, the simulations of bilayers with a neutral group implementation do not suffer greatly from the omission of long-range electrostatics.[32] This observation suggests that our MRI water model could be accurate enough for the bilayer simulation.

An appropriate scheme for simulating the bilayer in MRI water is sketched in Figure 11. More specifically, water−water interactions were treated using the MRI/GC/0.7 model and the slt/blk scheme with $R_{cut}^{slt} = 0.6$ nm, as described in Section 4.1. The MS-CG/GC one-site water potential was recalculated for this simulation, using a fit to the water subsystem of the atomistic bilayer, and is, therefore, slightly different from the MS-CG/GC bulk potential studied in Section 3.1. One important difference is that the TIP3P potential in the bilayer simulation sets Lennard-Jones interactions for hydrogen to zero. The polarized (more ordered) water structure near the bilayer is a second major factor. Similar to the MRI modeling of ionic solutions, lipid−water interactions in the MRI modeling here were described atomistically with cutoff electrostatics using the FM correction, with $R_{cut} = 0.9$ nm (see Figure 11). In this particular simulation geometry, about 30% of water−water pairs interacted through the MRI potential. The Ewald method was used to evaluate the electrostatic contribution to lipid−lipid interactions and can be considered accurate due to the overall neutrality of the lipid subsystem.

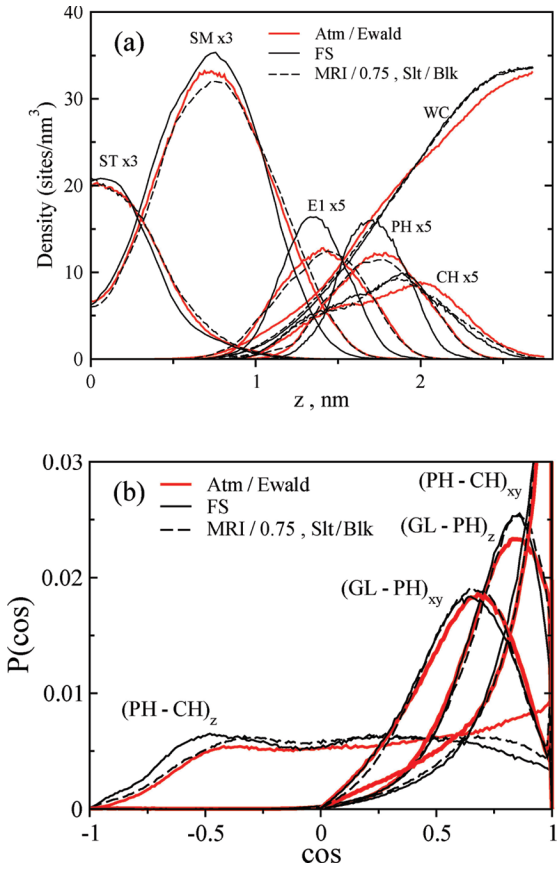

Figure 12. Structure of the DMPC bilayer determined using atomistic Ewald (red), FS (solid thin), and MRI/0.75 with slt/blk water (dashed) simulations. (a): Bilayer normal density profiles of lipid groups and water (CM). (b): Distributions of the normal (*z*) and in-plane (*xy*) components of vectors connecting headgroup sites, PH−CH and GL−PH. The partitioning of a DMPC molecule into CG groups is shown in Figure 11. The symbols are: CH, choline moiety; PH, phosphate group; GL, glycerol backbone; E1, ester group at *sn* − 1 chain; and SM/ST, three-carbon groups of the acyl chains.

A comparison of the reference atomistic simulation using the Ewald method, the MRI simulation, and an atomistic MD simulation using the FS cutoff (R_{cut} = 1.0 nm) is shown in Figure 12. In Figure 12a, we compare the density profiles of water and lipid groups, in accordance with the partitioning adopted in ref 7 and shown in Figure 11. Figure 12b compares the distributions of normal and in-plane group orientations obtained by the three simulations. Note that the FS cutoff and Ewald simulations produced very different normal density distributions. In the cutoff simulation, the DMPC density of headgroup sites was more localized, and the water also penetrated less into the headgroup region, resulting in a lower water density outside the center of the water region. This water density profile is consistent with a positive lateral pressure at the center of the water region.[33] The lower hydration level of headgroups in the cutoff simulation (compared to the Ewald simulation) affected bilayer properties, such as equilibrium area per lipid. The MRI water density follows virtually the same pattern. Thus, it is fair to say that the loss of medium- and long-ranged lipid−water and water−water interactions causes weaker hydration of hydrophilic lipid sites in both the cutoff and MRI simulations.

A surprising result is that the MRI simulation reproduced the normal density of headgroup sites much better than that of the FS cutoff simulation. This advantage is likely a result of using the Ewald method to treat electrostatics within the lipid subsystem. The headgroup orientations were also slightly more accurate in the MRI simulation than in the FS cutoff simulation. For example, the distribution of the normal component of PH−CH was in better agreement with the Ewald results. This result is important, as the normal component of the interaction between headgroup dipoles is strong.

5. Conclusions

In this paper a novel mixed resolution interaction (MRI) method has been proposed that combines atomistic and coarse-grained (CG) descriptions of molecular interactions in condensed-phase systems. The method defines the mixed resolution interactions only along the pairwise interactions between particles and not at space-fixed boundaries in the simulation cell like other mixed resolution approaches. The total forces acting on individual atoms in the MRI framework include both accurate atomistic contributions arising from nearby molecules and from "unfolded" forces derived from the molecular MS-CG forces between pairs of distant molecules. We have also introduced a transition region between the atomistic and CG zone, which smoothes the forces. The MS-CG force fields, described fully elsewhere, are based on a preselected partitioning of the system into CG units and have been previously shown to properly incorporate many-body effects.

Implementation of the MRI algorithm involves a CG group-based cutoff treatment of interactions, similar to the neutral group implementation used in cutoff electrostatics. A group-based cutoff formalism is computationally more demanding than a simple cutoff treatment. However, as atomistic interactions outside the relative small atomistic zone are still derived from the MS-CG forces through the computationally cheap unfolding scheme mentioned above, the MRI simulations will lead to significantly improved computational performance, especially for very large systems.

The MRI methodology was applied to both liquid water and methanol, both of which are important solvents. With a sufficiently large atomistic zone, it was possible to achieve a description of water properties superior to that provided by simple cutoff methods. The MRI description of liquid methanol resulted in good liquid structure, but thermodynamic and diffusion properties were reproduced less accurately. This deficiency may be attributable to the bulkier methanol molecules or to the inaccuracy of the one-site CG methanol model. For both water and methanol, the MRI modeling is likely to be improved, if the underlying CG model is made to be more thermodynamically and structurally accurate.

The transferability of the MRI water potentials to inhomogeneous environments, however, appears to be more challenging. For an aqueous ion solution, the MRI treatment of water−water interactions led to unnatural stability in the

ionic complexes. This artifact can be attributed to the fact that water−water interactions are effectively different in the environment perturbed by the ionic solutes. To improve the dynamics of the ionic solute association, we added an atomistic description of the interactions among water molecules within a preselected radius of the solutes. This approach, denoted the solute/bulk (slt/blk) scheme, proved to be effective and is expected to perform even better for systems with a larger water subsystem (for example, solvated proteins). We also tested a computationally less-expensive algorithm for correcting the interactions in perturbed water, where atomistic potentials are used only if both water molecules belong to solute neighborhoods. However, this approach proved insufficient to correctly simulate solute association dynamics. Finally, the MRI description of water−water interactions with the solute/bulk enhancement was applied with reasonable success to simulate a phospholipid bilayer, where the electrostatic interactions within the bilayer subsystem were evaluated using accurate Ewald summation.

The advance described in this paper on mixed resolution modeling must be considered preliminary. Clearly, the MRI method does not always perform well for heterogeneous systems, though likely it is better than purely coarse-grained modeling of similar systems. Moreover, the fully efficient and optimized computational implementation of the MRI method remains for future work. Nevertheless, the overarching concept of the MRI approach is a novel one that changes resolution of the interactions as a function of only the interparticle separation and not in terms of regions fixed in space.

Acknowledgment. The research was supported by the National Science Foundation (CHE-0719522) and the Office of Naval Research.

Supporting Information Available: Properties of bulk TIP3P water at ambient conditions, as determined from MRI/GC simulations with dipole (first line of data for each property) and Coulomb (second line) unfolding schemes for various atomistic zone sizes R_{atm}, and an Ion-water structure for a 12 ion system in 1 500 water molecules. This material is available free of charge via the Internet at http://pubs.acs.org.

References

(1) Noid, W. G.; Ayton, G. S.; Izvekov, S.; Voth, G. A. The Multiscale Coarse-Graining Method: A Systematic Approach to Coarse Graining. In *Coarse-graining of condensed-phase and biomolecular systems*; Voth, G. A., Ed.; CRC Press/Taylor and Francis Group: Boca Raton, FL, 2009; pp 21.

(2) Shelley, J. C.; Shelley, M. Y.; Reeder, R. C.; Bandyopadhyay, S.; Klein, M. L. *J. Phys. Chem. B* **2001**, *105*, 4464.

(3) Marrink, S. J.; Mark, A. E. *J. Am. Chem. Soc.* **2003**, *125*, 15233.

(4) Marrink, S. J.; de Vries, A. H.; Mark, A. E. *J. Phys. Chem. B* **2004**, *108*, 750.

(5) Tozzini, V. *Curr. Opin. Struct. Biol.* **2005**, *15*, 144.

(6) Lyubartsev, A. P.; Laaksonen, A. *Phys. Rev. E: Stat. Phys., Plasmas, Fluids, Relat. Interdiscip. Top.* **1995**, *52*, 3730.

(7) Izvekov, S.; Voth, G. A. *J. Phys. Chem. B* **2005**, *109*, 2469.

(8) Izvekov, S.; Voth, G. A. *J. Chem. Phys.* **2005**, *123*, 134105.

(9) Izvekov, S.; Voth, G. A. *J. Chem. Theory Comput.* **2006**, *2*, 637.

(10) Ayton, G. S.; Noid, W. G.; Voth, G. A. *Mat. Res. Bull.* **2007**, *32*, 929.

(11) Zhou, J.; Thorpe, I. F.; Izvekov, S.; Voth, G. A. *Biophys. J.* **2007**, *92*, 4289.

(12) Liu, P.; Izvekov, S.; Voth, G. A. *J. Phys. Chem. B* **2007**, *111*, 11566.

(13) Noid, W. G.; Chu, J. W.; Ayton, G. S.; Voth, G. A. *J. Phys. Chem. B* **2007**, *111*, 4116.

(14) Noid, W. G.; Chu, J.-W.; Ayton, G. S.; Krishna, V.; Izvekov, S.; Voth, G. A.; Das, A.; Andersen, H. C. *J. Chem. Phys.* **2008**, *128*, 244114.

(15) Noid, W. G.; Liu, P.; Wang, Y.; Chu, J.-W.; Ayton, G. S.; Izvekov, S.; Andersen, H. C.; Voth, G. A. *J. Chem. Phys.* **2008**, *128*, 244115.

(16) Praprotnik, M.; Site, L. D.; Kremer, K. *J. Chem. Phys.* **2005**, *123*, 224106.

(17) Christen, M.; van Gunsteren, W. F. *J. Chem. Phys.* **2006**, *124*, 154106.

(18) Praprotnik, M.; Site, L. D.; Kremer, K. *Phys. Rev. E: Stat. Phys., Plasmas, Fluids, Relat. Interdiscip. Top.* **2006**, *73*, 066701.

(19) Praprotnik, M.; Kremer, K.; Site, L. D. *Phys. Rev. E: Stat. Phys., Plasmas, Fluids, Relat. Interdiscip. Top.* **2007**, *75*, 017701.

(20) Praprotnik, M.; Site, L. D.; Kremer, K. *J. Chem. Phys.* **2007**, *126*, 134902.

(21) Praprotnik, M.; Kremer, K.; Site, L. D. *J. Phys. A: Math. Theor.* **2007**, 40.

(22) Ensing, B.; Nielsen, S. O.; Moore, P. B.; Klein, M. L.; Parrinello, M. *J. Chem. Theory Comput.* **2007**, *3*, 1100.

(23) Delle Site, L. *Phys. Rev. E: Stat. Phys., Plasmas, Fluids, Relat. Interdiscip. Top.* **2007**, *76*, 047701.

(24) Errington, J. R.; Debenedetti, P. G. *Nature* **2001**, *409*, 318.

(25) Izvekov, S.; Swanson, J. M. J.; Voth, G. A. *J. Phys. Chem. B* **2008**, *112*, 4711.

(26) Matysiak, S.; Clementi, C.; Praprotnik, M.; Kremer, K.; Site, L. D. *J. Chem. Phys.* **2008**, *128*, 24503.

(27) Jorgensen, W. L.; Maxwell, D. S.; Tirado-Rives, J. *J. Am. Chem. Soc.* **1996**, *118*, 11225.

(28) Hummer, G.; Pratt, L. R.; Garcia, A. E. *J. Phys. Chem.* **1996**, *100*, 1206.

(29) Smondyrev, A. M.; Berkowitz, M. L. *J. Comput. Chem.* **1999**, *20*, 531.

(30) Darden, T.; York, D.; Pedersen, L. *J. Chem. Phys.* **1993**, *98*, 10089.

(31) Ayton, G.; Smondyrev, A. M.; Bardenhagen, S. G.; McMurtry, P.; Voth, G. A. *Biophys. J.* **2002**, *83*, 1026.

(32) Wohlert, J.; Edholm, O. *Biophys. J.* **2004**, *87*, 2433.

(33) Lindahl, E.; Edholm, O. *J. Chem. Phys.* **2000**, *113*, 3882.

CT900414P